AGU PUBLICATIONS

JGR

Journal of Geophysical Research: Atmospheres

RESEARCH ARTICLE
10.1002/2015JD024099

Key Points:
- Subcanopy incoming longwave radiation was modeled at three alpine sites
- Errors arose from the assumption that air temperature is the same as canopy temperature
- Estimates were improved by subdividing the canopy into two emitting components

Correspondence to:
C. Webster,
clare.webster@northumbria.ac.uk

Citation:
Webster, C., N. Rutter, F. Zahner, and T. Jonas (2016), Modeling subcanopy incoming longwave radiation to seasonal snow using air and tree trunk temperatures, *J. Geophys. Res. Atmos.*, *121*, doi:10.1002/2015JD024099.

Received 17 AUG 2015
Accepted 19 DEC 2015
Accepted article online 23 DEC 2015

Modeling subcanopy incoming longwave radiation to seasonal snow using air and tree trunk temperatures

Clare Webster[1,2], Nick Rutter[1], Franziska Zahner[2,3], and Tobias Jonas[2]

[1]Department of Geography, Faculty of Engineering and Environment, Northumbria University, Newcastle Upon Tyne, UK, [2]WSL Institute for Snow and Avalanche Research SLF, Davos Dorf, Switzerland, [3]Institute of Environmental Engineering, ETH Zurich, Zurich, Switzerland

Abstract Data collected at three Swiss alpine forested sites over a combined 11 year period were used to evaluate the role of air temperature in modeling subcanopy incoming longwave radiation to the snow surface. Simulated subcanopy incoming longwave radiation is traditionally partitioned into that from the sky and that from the canopy, i.e., a two-part model. Initial uncertainties in predicting longwave radiation using the two-part model resulted from vertical differences in measured air temperature. Above-canopy (35 m) air temperatures were higher than those within (10 m) and below (2 m) canopy throughout four snow seasons (December–April), demonstrating how the forest canopy can act as a cold sink for air. Lowest model root-mean-square error (RMSE) was using above-canopy air temperature. Further investigation of modeling subcanopy longwave radiation using above-canopy air temperature showed underestimations, particularly during periods of high insolation. In order to explicitly account for canopy temperatures in modeling longwave radiation, the two-part model was improved by incorporating a measured trunk view component and trunk temperature. Trunk temperature measurements were up to 25°C higher than locally measured air temperatures. This three-part model reduced the RMSE by up to 7.7 W m^{-2} from the two-part air temperature model at all sensor positions across the 2014 snowmelt season and performed particularly well during periods of high insolation when errors from the two-part model were up to 40 W m^{-2}. A parameterization predicting tree trunk temperatures using measured air temperature and incoming shortwave radiation demonstrate a simple method that can be applied to provide input to the three-part model across midlatitude coniferous forests.

1. Introduction

Snowmelt-dominated forested headwater catchments produce up to 60% of global freshwater runoff [*Chang*, 2003]. The understanding of interactions between forested environments and seasonal snow cover is therefore important for accurate snowmelt predictions. Snowmelt in forest environments contributes substantially to the timing and quantity of spring surface runoff and is largely controlled by the local surface radiation budget, which can account for up to 80% for the total energy available for snowmelt [*Link and Marks*, 1999; *Marks and Dozier*, 1992]. In midlatitude forested regions, the shading, reflection, absorption, and emission of incoming shortwave and longwave radiation causes significant spatial and temporal differences in the surface energy balance within forests relative to adjacent open areas [*Harding and Pomeroy*, 1996; *Hardy et al*., 1998; *Lundquist et al*., 2013; *Rowlands et al*., 2002].

Above the canopy and under clear-sky conditions the dominant radiative flux is shortwave radiation, whereas under cloudy conditions, close to trees that receive a high amount of shortwave radiation, or in dense canopies, the longwave component can contribute similar or larger amounts of radiation to the snow surface [*Lawler and Link*, 2011; *Sicart et al*., 2006]. In particular, the increased temperature of the canopy compared to the air results in positive longwave radiation fluxes below the canopy compared to negative fluxes in adjacent open areas [*Lundquist et al*., 2013], which subsequently has implications for snowmelt and snow disappearance date. During the snowmelt period the presence of forest can lead to enhanced melt as the total contribution of longwave radiation increases, particularly in midlatitude environments where daytime temperatures increase above 0°C [*Lundquist et al*., 2013]. This phenomenon is particularly prevalent in canopy discontinuities where there is heightened exposure to solar radiation and increased emission of longwave radiation from heated canopy elements [*Lawler and Link*, 2011; *Seyednasrollah and Kumar*, 2014]. As solar angles and incoming shortwave radiation increase through the snowmelt period, the formation of tree wells in forest environments and

the subsequent retreat of the snowline away from forest edges indicate a preferential melt profile close to tree trunks [*Pomeroy et al*., 2009; *Woo and Giesbrecht*, 2000]. *Lawler and Link* [2011] identified radiative "hot spots" on the northern edges of gaps, where both the measured longwave and shortwave radiation was at maxima within 1–2 m of the forest edge. In particular, measured incoming longwave radiation at these locations was up to 50 W m^{-2} higher than that measured on the southern edge of these gaps. Furthermore, modeling results at the northern edges of gaps showed an underestimation of incoming longwave radiation during daytime and an overestimation during nighttime, indicating the influence of sunlit forest canopy areas on storage and subsequent emission of radiation to the nearby snow surface. The effect of these heated canopy elements remains a source of uncertainty when modeling incoming longwave radiation dynamics within discontinuous canopies [*Ellis et al*., 2010; *Lawler and Link*, 2011]. In particular, the assumption that a single air temperature can be used to represent that of the entire canopy remains a limitation in both local and distributed incoming longwave radiation modeling [*Pomeroy et al*., 2009; *Seyednasrollah and Kumar*, 2014].

This study uses data collected in the central Swiss Alps between 2004 and 2014 to investigate the performance of subcanopy incoming longwave radiation models driven by air and canopy temperatures. The aim of this paper is to assess the current methods to model incoming longwave radiation below the forest canopy, specifically (1) the use of measured air temperature (both above, within and below the canopy) as a proxy for canopy temperature in closed-canopy environments and (2) the addition of a measured trunk view fraction and trunk temperature to better represent the different canopy elements comprising the total hemispherical view.

2. Modeling Incoming Longwave Radiation

Incoming longwave radiation from the sky is calculated by

$$\downarrow \mathrm{LW} = \sigma \varepsilon_{\mathrm{sky}} T_{\mathrm{air}}^4 \tag{1}$$

where σ is the Stefan-Boltzmann constant (5.67×10^{-8} W m^{-2} K^{-4}), T is the temperature of the air (K), and $\varepsilon_{\mathrm{sky}}$ is the dimensionless effective emissivity of the sky which varies between 0.7 and close to one depending on cloud cover [e.g., *Essery et al*., 2008; *Flerchinger et al*., 2009; *Gubler et al*., 2012].

Addition of forest canopy extends equation (1) into a two-part model through the division of the hemispherical view into sky view fraction (V_f) and canopy view fraction ($1 - V_f$):

$$\downarrow \mathrm{LW} = V_f \left(\sigma \varepsilon_{\mathrm{sky}} T_{\mathrm{sky}}^4 \right) + (1 - V_f)\left(\sigma \varepsilon_{\mathrm{can}} T_{\mathrm{can}}^4 \right) \tag{2}$$

where T_{can} and $\varepsilon_{\mathrm{can}}$ are the temperature and emissivity of the canopy, respectively. Canopy emissivity values used in previous studies vary between 0.9 and 1 [*Essery et al*., 2008; *Liston and Elder*, 2006; *Pomeroy et al*., 2009; *Price and Petzold*, 1984; *Woo and Giesbrecht*, 2000]. Modeling in this study used a value of 0.98 for $\varepsilon_{\mathrm{can}}$.

The sky component of incoming longwave radiation can be replaced by a measured value either above the canopy or at a nearby open site:

$$\downarrow \mathrm{LW} = V_f \mathrm{LW}_{\mathrm{sky}} + (1 - V_f)\left(\sigma \varepsilon_{\mathrm{can}} T_{\mathrm{can}}^4 \right) \tag{3}$$

where $\mathrm{LW}_{\mathrm{sky}}$ in this case is the measured incoming longwave radiation from the sky. Modeling by *Essery et al*. [2008] showed that calculating the $\mathrm{LW}_{\mathrm{sky}}$ component of equation (3) results in larger errors in estimates of incoming longwave radiation below the canopy than when using a measured value. Therefore, modeling in this present study used a measured value for $\mathrm{LW}_{\mathrm{sky}}$ in order to specifically assess errors in incoming longwave radiation resulting from using air or canopy temperatures.

Previous studies using equation (2) or (3) have assumed $T_{\mathrm{can}} = T_{\mathrm{air}}$ [e.g., *Essery et al*., 2008; *Lawler and Link*, 2011; *Sicart et al*., 2004], as T_{air} is comparatively easier to measure and more readily available. This assumption has been found to be accurate in dense canopies, at low Sun angles or under cloudy conditions. However, *Sicart et al*. [2004] showed, across a 20 day period, that the movement of air below the canopy leads to vertical differences in air temperature. In larger-scale atmospheric snowmelt models, the reference canopy temperature is often taken to be the temperature of the lower atmosphere, a local air temperature measured above the canopy, or in a local open site. *Pomeroy et al*. [2009] found that the air temperature above a discontinuous canopy was similar to measured tree needle temperature below the canopy. This study will further investigate these findings by modeling subcanopy incoming longwave radiation using above, within, and below

canopy measured air temperature across multiple snowmelt seasons with the objective of determining whether above-canopy temperatures can be used as a proxy for below-canopy temperatures.

A further limitation of equations (2) and (3) and the assumption that $T_{can} = T_{air}$ is that high insolation in forest discontinuities causes the temperature of the canopy, particularly the woody elements, to increase up to 25°C higher than the surrounding air temperature [*Howard and Stull*, 2013; *Pomeroy et al*., 2009] (cf. Figure 6). Model-based studies have since partitioned the canopy into two theoretical emitting components: trunk and remainder of canopy (i.e., leaves, needles, and branches), with the argument that they have different thermal regimes due to the differences in surface area and volume [*Gouttevin et al*., 2015; *Seyednasrollah and Kumar*, 2013]. However, these studies did not directly measure canopy temperatures and instead estimated them based on other measured parameters. While these findings suggest a relationship between incoming longwave radiation energy and the trunk view component of the hemispherical view and its temperature, this has yet to be tested with field-based measurements of trunk view fraction (TV_f) and its temperature. Consequently, a further component of the hemispherical view is proposed so that the canopy is divided into two separate components (tree trunk and remainder of canopy) with separate temperatures, thus extending equation (3) into a three-part model (equation (4)). Direct measurement of TV_f, determined by hemispherical photography, and the remainder of the canopy ($1 - V_f - TV_f$) calculated as the remainder of the total hemispherical view, is used in:

$$\downarrow LW = V_f LW_{sky} + TV_f\left(\sigma\varepsilon_{tree}T_{tree}^4\right) + (1 - TV_f - V_f)\left(\sigma\varepsilon_{can}T_{can}^4\right) \quad (4)$$

Thermal photography from this study (cf. Figure 6) and previous results from *Sicart et al*. [2004] and *Pomeroy et al*. [2009] suggest that temperature of remainder of the canopy (T_{can}) can be substituted by the measured local air temperature. In this study, both the TV_f and temperature of the tree trunk (T_{tree}) are directly measured.

Pomeroy et al. [2009] showed that during high insolation, tree trunk temperatures were greater than measured air temperatures across three three-day measurement periods. A simple parameterization to predict tree trunk temperatures from knowledge of incoming shortwave radiation and air temperature is proposed:

$$\delta T = T_{air} + \left(a^* \downarrow SWR + b\right) \quad (5)$$

where δT (°C) is the difference between trunk and air temperatures ($T_{tree} - T_{air}$), $\downarrow$SWR is measured incoming shortwave radiation (W m^{-2}) at the base of the tree trunk, and a and b are regression coefficients. This study used measured values of T_{air} and $\downarrow$SWR to parameterize a function to predict δT (cf. section 5.3).

3. Field Sites

Data collected at three forested field sites in the Swiss Alps (Figure 1) were used for analysis of air and canopy temperatures and incoming longwave radiation modeling (summarized in Table 1). The combination of all data collected at these sites across a combined period of 11 years (2004–2014) allows a comprehensive assessment of the performance of air and canopy temperatures on subcanopy incoming longwave radiation modeling.

The first two of these, Alptal and Seehornwald, are established field sites by the Swiss Federal Institute for Forest, Snow and Landscape Research WSL. Alptal is in a subalpine forested valley located in central Switzerland (47°03′N, 8°43′E) at approximately 1220 m above sea level (asl) (Figure 1a). Norwegian Spruce trees dominate the forest and are typically 25 m high. Temperature and model validation data used in this study were collected between January 2004 and April 2007. Seehornwald is located close to the city of Davos in eastern Switzerland (46°48′55″N, 9°51′21″E) at 1640 m asl (Figure 1b). Seehornwald is also Norwegian Spruce dominated and tree heights reach 27 m. Temperature and model validation data used in this study were collected between January 2008 and May 2014.

The third field site was located in a discontinuous Norwegian Spruce dominated forest close to Davos Laret (Figure 1b) at 1520 m asl in eastern Switzerland (46°50′42″N, 9°52′19″E). Data collected at this site throughout the 2014 winter is summarized in the following section.

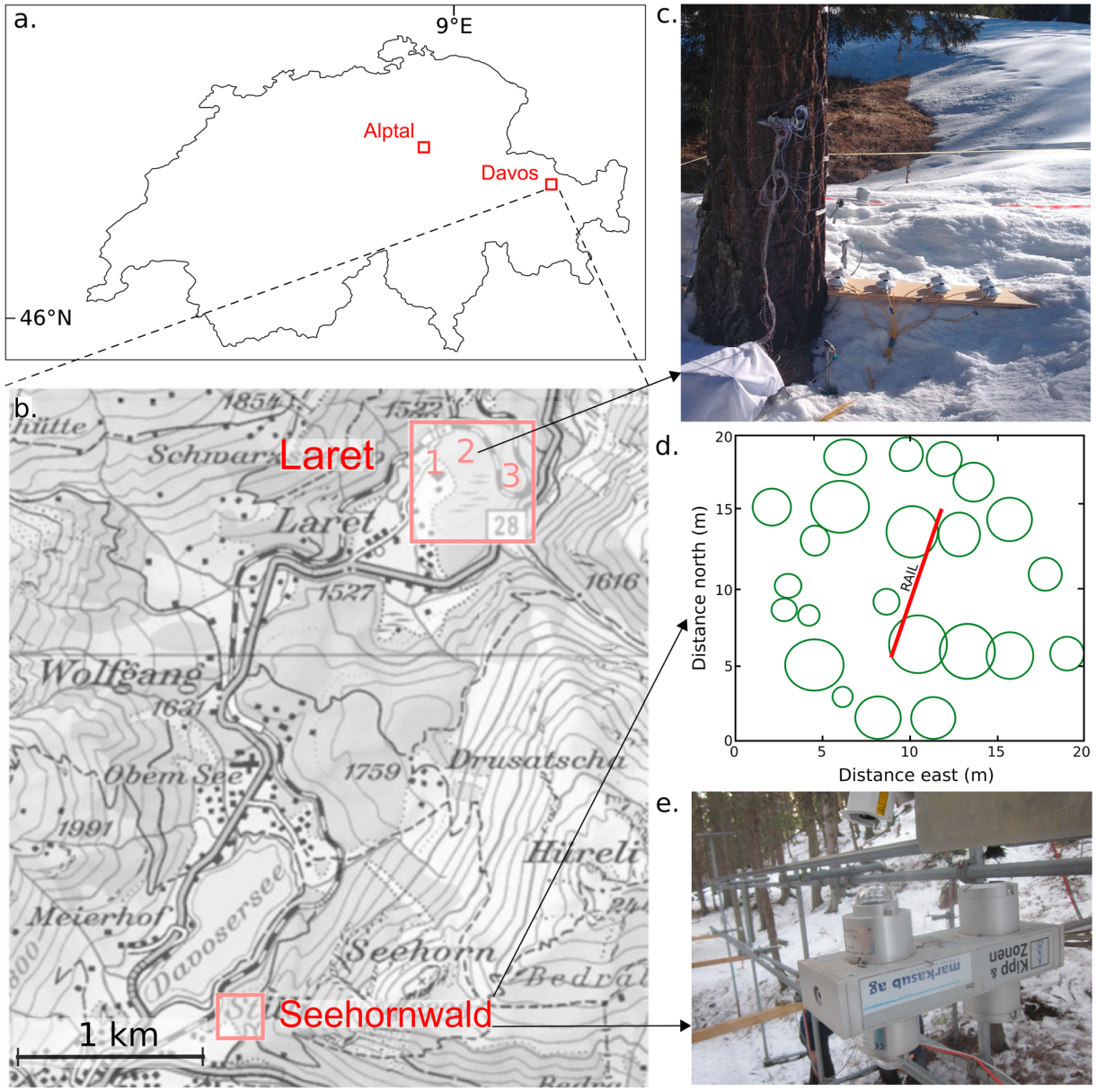

Figure 1. Overview of field locations and setup. (a) Location map showing all Swiss subalpine field sites used in this study, including Alptal and Davos (Seehornwald and Laret). (b) Overview of Davos area showing proximity of Seehornwald and Laret; Laret inset shows location of (1) open site, (2) Tree 1, and (3) Tree 2. (c) Radiometer and tree temperature setup for Tree 2 at Laret where radiometer pairs are spaced on a wooden plank south of the tree, thermocouples are connected to the tree bark, and infrared thermocouples are at radiometer height either side of the wooden plank; the setup was the same for Tree 2 at Laret. (d) Bird's-eye view of the Seehornwald site showing location of rail relative to trees, green circles represent tree crown positions determined by aerial lidar data. (e) Photograph looking southwest showing the rail and CNR1 setup; the rail and CNR1 setup was identical for Alptal.

Table 1. Data Summary of Swiss Subalpine Forested Field Sites With Links to Associated Objectives and Equations[a]

	Elevation	V_f Range	Dates	Data	Data Resolution	Equation (Number)
Alptal	1220 m	0.09–0.18	January 2004 to May 2007	SW, LW, V_f, T_{air} (2, 10, and 35 m)	1 min	Two-part model (3)
Seehornwald	1640 m	0.02–0.05	December 2008 to May 2014	SW, LW, V_f, T_{air} (35 m)	15 s,	Two-part model (3)
Laret	1520 m	0.38–0.50 (T1)	January 2014 to April 2014	SW, LW, V_f, TV_f, T_{air} (1 m), T_{tree}	10 min	Two-part model (3)
		0.15–0.20 (T2)				Three-part model (4)

[a]Sky view fraction (V_f) range for all sites including Tree 1 (T1) and Tree 2 (T2) at Laret. Data availability includes shortwave (SW) and longwave (LW) radiation, air and tree temperatures (T_{air} and T_{tree}), and trunk view fraction (TV_f).

4. Data Collection

4.1. Alptal and Seehornwald

Incoming shortwave and longwave radiation at the Alptal and Seehornwald sites were measured using Kipp and Zonen CNR1 net radiometer sensors mounted on a moving rail below the canopy and on static cross arms on top of a tower above the canopy. The CNR1 consists of two CM3 pyranometers and two CG3 pyrgeometers, which are the predecessors of the CGR3 and CMP3 radiometers used at the Laret field site with very similar characteristics. Incoming shortwave and longwave radiation were measured simultaneously at 1 min (Alptal) and 15 s (Seehornwald) resolution. Details of the rail-mounted radiometers are described in *Stähli et al*. [2009] and *Webster et al*. [2015] and were replicated when the equipment was moved from Alptal to the Seehornwald site in 2007. The subcanopy CNR1 moved along a 10 m heated rail at 10 min intervals at a constant velocity and at a height of approximately 2 m above the forest floor, covering a range of V_f (Alptal: 0.09–0.18; Seehornwald; 0.02–0.05). Air temperature measurements were taken above the canopy at 35 m at both sites. Additional air temperature measurements below (2 m) and within (10 m) the canopy were available for the Alptal site. From 2010 onward, a brush was installed to clear intercepted snow on the up-looking rail-mounted sensors below the canopy at Seehornwald, thus allowing a continuous time series. For data collected before the addition of the cleaning brush, when interception was present on the sensors, data were manually removed in postprocessing. Additionally, when snow had accumulated on the pyranometer and pyrgeometer on the tower above the canopy, data were again manually removed in postprocessing.

Radiation data collected using the two CNR1 net radiometers at Alptal (2004–2007) followed factory calibration specifications. Outdoor recalibration of all eight individual pyranometers and pyrgeometers on the two CNR1 net radiometers was carried out in August 2013 by the World Radiation Center (WRO) in Davos, Switzerland to WRO standards [*Fröhlich*, 1977]. Data from Seehornwald (2008–2014) were recalculated using the individual channel WRO-calibrated specifications.

Data collected at Alptal and Seehornwald between 2004 and 2014 were used to evaluate the effect of vertical air temperature profiles (Alptal) and above-canopy air temperatures (Seehornwald) on estimates of subcanopy incoming longwave radiation throughout 10 complete snowmelt seasons. The availability of vertical air temperature profile data at Alptal allowed the investigation into the extent to how air temperatures differ through different heights below, within, and above the canopy. These air temperature data were further used in the two-part model (equation (3)) to model subcanopy incoming longwave radiation. Further long-term modeling of subcanopy incoming longwave radiation was carried out using data collected between 2008 and 2014 at Seehornwald. This data were collected at a higher resolution (15 s) than at Alptal (1 min) and the presence of the brush from 2010 onward made a larger amount of data available for validation of the two-part model. Type T contact thermocouples were also installed at the tree in Seehornwald, at the north-eastern end of the rail (Figure 1e), between 26 January to 26 February and 3–11 April 2014. Twenty-one pairs were installed between 1 and 3 m from the canopy floor 360° around the tree trunk.

4.2. Laret

Incoming shortwave and longwave radiation was investigated at Laret between February and April 2014 at two separate trees of different species and positions within the forest (Figure 1b). A larch tree (herein after referred to as Tree 1) located on the northern edge of a large gap was studied between 7 and 26 February. A conifer (Tree 2) located on the northern side of a smaller forest discontinuity was studied between 26 February and 11 March (installation 1), and again between 16 and 29 April (installation 2). At each tree, incoming radiation was measured using four pairs of Kipp and Zonen CMP3 pyranometers and CGR3 pyrgeometers arranged linearly radiating south from the study tree (Figure 1c). Between 7 and 20 February, the sensors were arranged at 15 cm intervals away from the tree. From 20 February until the end of the snowmelt period (29 April), sensors were located 30 cm apart, ranging between 7 cm and 97 cm from the trunk in order to better capture the spatial variation in incoming longwave radiation with increasing distance from the tree trunk. These distances were experimentally determined, covering a range radiating from the tree trunk up to the point at which incoming longwave radiation showed no noticeable decrease. This change in sensor arrangement divides the period at Tree 1 into two installations (installation 1: 7–20 February and installation 2: 20–26 February). A CMP3/CGR3 pair was also located in a nearby open site (Figure 1), which was taken to represent above-canopy conditions.

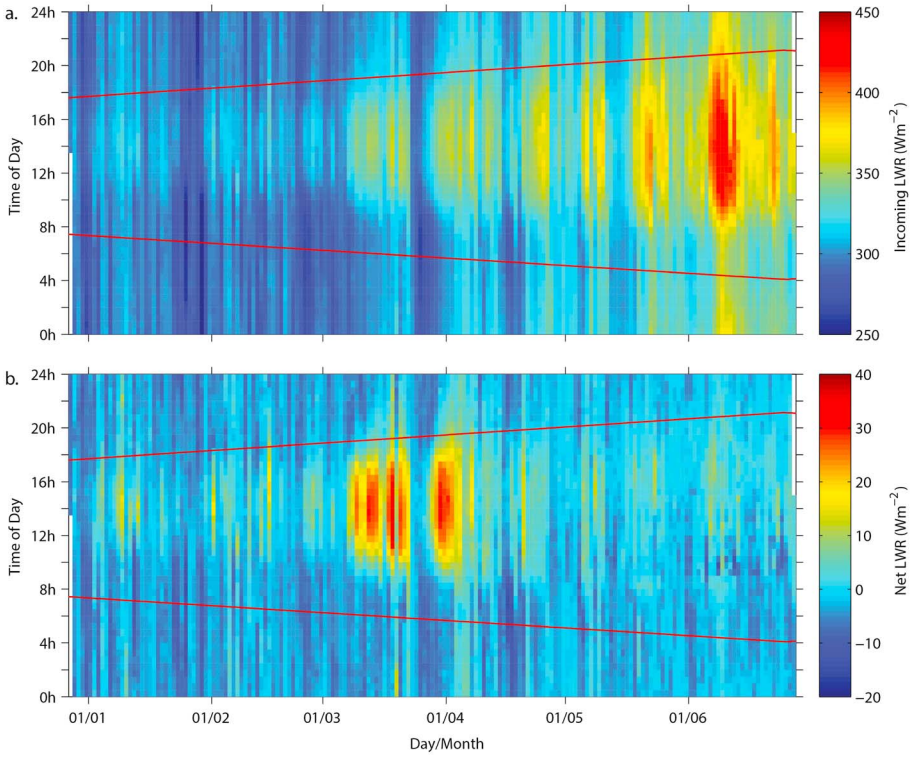

Figure 2. Hourly averaged subcanopy (a) incoming longwave radiation and (b) net longwave flux (incoming-outgoing) collected along the 10 m rail at Seehornwald between December 2013 and May 2014 (*x* axis) for time of day (*y* axis). Bold red lines show time of sunrise and sunset.

All sensors were connected to Campbell Scientific CR1000 data loggers, recording at 15 s intervals and averaged to 10 min. Each radiometer was placed on a rigid wooden platform and leveled and cleared of any accumulation of fresh snow or ice, once in the morning during the accumulation period, and twice daily (in the morning and at midday) during snowmelt. Periods of data when the sensors were snow covered, being cleared, or significantly tilted due to uneven depletion of the snow surface were removed in postprocessing.

Both air and tree temperatures were measured during all installations. Air temperature was measured at 1 m above the snow surface, both at the trees and at the open site, using a T107 thermistor housed in a radiation shield. Tree trunk temperature was measured using two methods: (1) six pairs of Type T contact thermocouples (TCs), consisting of copper and constantan conductors were embedded just below the bark surface on the south side of each tree; (2) two Campbell Scientific IR100 infrared temperature sensors (IRTCs) were pointed directly at the tree bark at the same height as the pyrgeometers. Tree temperature measurements using the IRTCs were unavailable for the second installation (16–29 April) at Tree 2. All tree temperature data were collected at 10 s intervals and averaged over 10 min intervals to be synchronous with radiation measurements. Additionally, values from the six thermocouple pairs and the pair of IRTCs were each averaged to obtain one trunk temperature value for each measurement method.

Thermal images of tree surface and canopy temperatures were taken using a VarioCAM® high-resolution inspect 768 (RE) Jenoptik thermal camera with an infrared image resolution of 1024 × 768 pixels. Images of Tree 1 were taken on 24 February in the late morning and early afternoon on a sunny day immediately following a snowfall event.

4.3. Calculation of V_f

In order to determine V_f and TV_f, hemispherical photographs were taken at each sensor location in Laret and at multiple positions along the rail in Alptal and Seehornwald. Photos were taken using a Canon 600D camera with a Sigma 4.5 mm F2.8 EX DC HSM fish-eye lens mounted on a metal plate that allowed easy leveling and orientation of the lens.

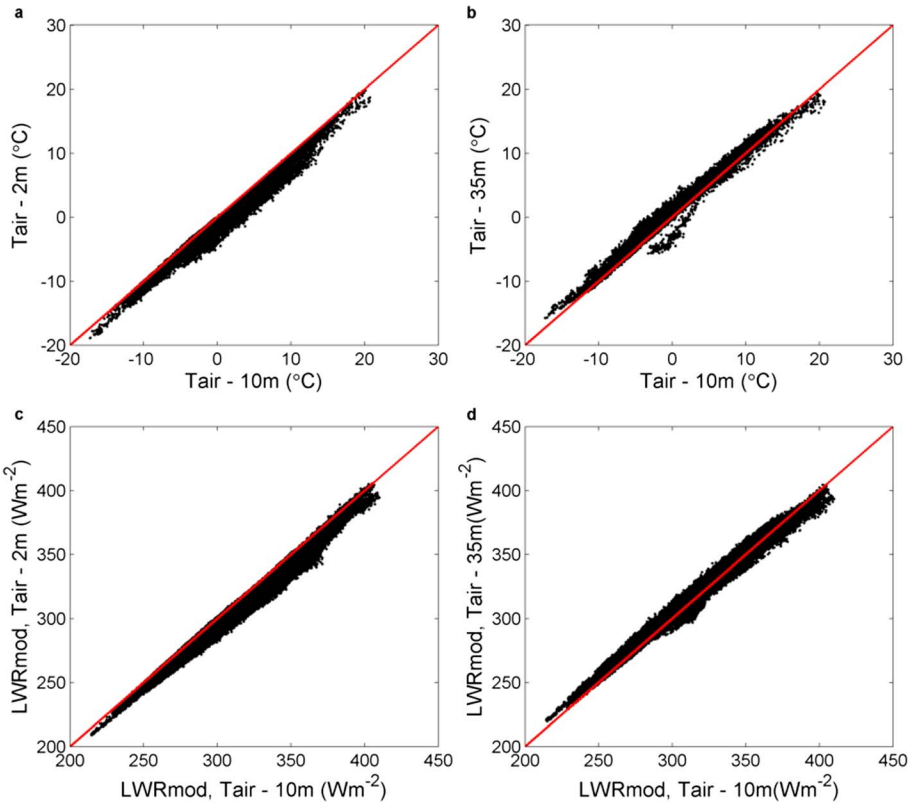

Figure 3. Difference in measured subcanopy air temperature at different heights within the canopy at the Alptal measurement site for (a) 10 m compared to 2 m, (b) 10 m compared to 35 m, and (c, d) the same for modeled results when using these air temperatures in equation (3).

Calculation of V_f was carried out by dividing the images into concentric rings based on elevation angle (θ) and pixels were classified into either white (sky) or black (canopy) using manual thresholding [*Reid and Essery*, 2013]. Sky view fraction was calculated from the ratio between numbers of sky and canopy pixels in each concentric ring, weighted by elevation angle according to *Essery et al.* [2008].

Hemispherical images taken at Laret were manually edited to distinguish the main tree trunk from the remainder of the canopy view. TV_f was manually calculated by selecting the region in the image that corresponds to the trunk view component of the hemispherical view, creating a binary image of "trunk" and "not trunk." Trunk view fraction was calculated following the same weighting procedure used in V_f calculations.

5. Results

5.1. Modeling Subcanopy Incoming Longwave Radiation Using Air Temperatures

Measured subcanopy incoming longwave radiation (hourly averages) is shown for 2014 at Seehornwald between December and June (Figure 2a). Diurnal patterns in longwave radiation show an asymmetrical pattern, with an increase from nighttime values around 10 A.M., between 2 and 3 h after sunrise, reaching a peak between 1 and 2 P.M., and returning to nighttime values after sunset (Figure 2a). Daily maximum values increased through the snowmelt period beginning mid-March, from 340 to 400 W m^{-2} at the end of April. These high levels of incoming longwave radiation also continued past sunset and on some days in April and May the values were still higher than 330 W m^{-2} after 8 P.M.. Corresponding subcanopy data on net longwave radiation (incoming-outgoing) are shown in Figure 2b, where red colors denote a net positive downwelling flux. Between mid-March (initiation of snowmelt) to the end of April (disappearance of snow), there was a positive net longwave radiation flux to the snow surface, reaching up to 40 W m^{-2} during the day (Figure 2b). This positive flux resulted from an increase in air and canopy temperatures, causing increased incoming longwave radiation to the snow surface, while at the same time the presence of snow cover

Table 2. Mean Model Bias (Modeled-Measured) and RMSE (Both W m^{-2}) of the Two-Part Model (Equation (3)) at Alptal Using Air Temperature Measured at Three Different Heights (2, 10, and 35 m) During December–May Between 2004 and 2007

	Mean Bias			RMSE		
	2 m	10 m	35 m	2 m	10 m	35 m
2004	−19.0	−15.6	−13.5	6.3	5.4	4.9
2005	−17.5	−13.7	−11.2	7.3	6.1	5.5
2006	−16.5	−12.7	−10.7	8.6	7.0	6.5
2007	−17.3	−11.4	−9.5	11.3	8.0	7.6

restricted the outgoing longwave radiative flux to a maximum of ~ 310 W m^{-2} (at an emitting temperature of 0°C). This one month demonstrates an optimum period for increased longwave energy at the melting snow surface compared to any other time during the 2014 winter snow season shown.

The influence of air temperature on modeling incoming subcanopy longwave radiation was evaluated across an 11 year period (2004–2014) at the Alptal and Seehornwald measurement sites. Air temperature at Alptal between 2004 and 2007 (January–April) varied between all three measurement heights (Figures 3a and 3b). Temporally coincident air temperature measurements were coldest at the 2 m measurement height (closest to the canopy floor), and warmest above the canopy at 35 m. The largest difference between temperatures measured below (2 m height) and within (10 m height) the canopy was 5.6°C, and the December–April mean was 1.1°C. Vertical differences in measured air temperature produced different estimations of incoming subcanopy longwave radiation (at the 2 m high rail) using the two-part model (equation (3)) (Figures 3c and 3d). Modeled values of subcanopy incoming longwave radiation at the rail using 10 m air temperature were almost always higher than when using the 2 m temperature and showed similar model results when using the 35 m temperature. Despite the similarities between the air temperature at 10 m and 35 m, the air temperature measured at 35 m resulted in the lowest mean bias and model root-mean-square error (RMSE) (Table 2) when used in the two-part model. Model bias and RMSE were highest using the 2 m air temperature, even though this was the height of the subcanopy pyrgeometer.

The assumption that air temperature can be used as a proxy for the emitting canopy temperature was further tested using the two-part model and data collected at the Seehornwald measurement site between 2008 and 2014, where continuous air temperature and subcanopy incoming longwave radiation data were available throughout all snow seasons (December to May). Mean air temperature between December and May during these years varied between −2.8 °C (2010) and 0.4 °C (2014). Seasonal RMSE for each of the seven years varied between 3.3 and 4.8 W m^{-2} (2013 and 2009, respectively) across the snowmelt seasons (Table 3). These RMSE were low relative to measurement error (±10%); however, individual bias values were greater than 40 W m^{-2}. Average model bias (modeled-measured) was negative in all months of all years, indicating underestimation of subcanopy incoming longwave radiation using above-canopy air temperature (Figure 4). The greatest model underestimations (>15 W m^{-2}) during the modeled snowmelt period were between late morning to middle afternoon in March–May, suggesting solar heating of the canopy was not represented by measured above-canopy air temperature. A comparison of model bias with above-canopy incoming shortwave radiation shows that overestimations (positive biases) decreased with increasing above-canopy shortwave radiation, particularly during April and May (Figure 4). During periods of high insolation, the two-part model underestimated the incoming longwave radiation by up to 15 W m^{-2}, particularly during April and May.

Table 3. Monthly (December–May) RMSE (W m^{-2}) Using the Two-Part Model (Equation (3)) at Seehornwald With Above-Canopy Air Temperature Between January 2008 and April 2014[a]

	Dec	Jan	Feb	Mar	Apr	May	Seasonal
2008	-	3.5	3.6	5.0	3.7	4.0	*4.1*
2009	5.2	6.0	4.3	4.7	3.6	4.4	*4.8*
2010	3.2	3.2	3.1	3.6	3.8	2.5	*3.4*
2011	2.7	3.4	3.7	4.0	4.2	4.2	*3.7*
2012	3.4	3.3	3.1	3.6	3.3	4.0	*3.5*
2013	3.6	2.9	2.9	3.4	3.7	2.1	*3.3*
2014	3.5	3.5	3.6	4.7	5.2	-	*4.3*
Monthly	*3.6*	*3.7*	*3.5*	*4.1*	*3.9*	*3.5*	

[a]Aggregate seasonal (Dec–May) and monthly RMSE are in italics.

The overestimations and underestimations shown through the interseasonal modeling at Seehornwald indicate that measured above-canopy air temperature did not closely match the canopy temperature as the assumption suggests. In general, the model underestimated subcanopy longwave radiation, suggesting that the temperature of the canopy was mostly higher than the measured air temperature above the canopy. Furthermore, overestimations (Figure 4) show that there were

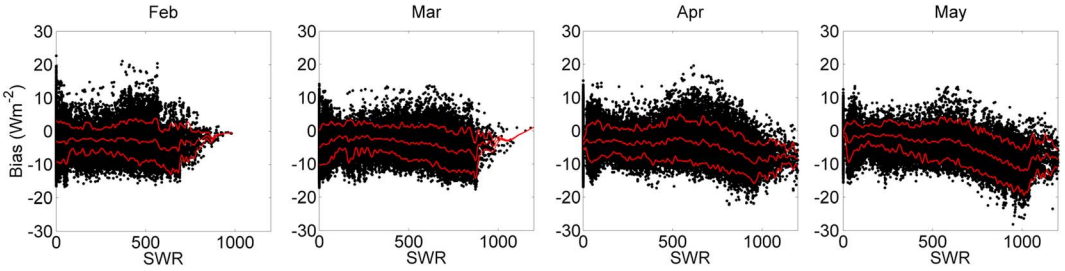

Figure 4. Monthly (February–May) relationship at Seehornwald between above-canopy incoming shortwave radiation and subcanopy longwave radiation model bias (modeled-measured) of equation (3) in 2011. Red lines indicate the median and upper and lower quartile ranges of model bias.

also periods when the emitting canopy temperature was lower than above-canopy air temperature. A comparison of tree and air temperatures at Seehornwald between 3 and 11 April indicates that air temperature was higher during the day, particularly between 12 and 6 P.M., whereas the tree trunk stayed warmer than the air temperature overnight (Figure 5). Seehornwald has a relatively closed canopy ($V_f = 0.02–0.05$), thus differences between canopy and above-canopy air temperatures are likely to be greater in sparse canopy environments with increased solar heating. These results suggest a need for explicit representations of canopy temperatures in subcanopy incoming longwave radiation models.

5.2. Modeling Subcanopy Incoming Longwave Radiation Using Canopy Temperatures

Data collected at Laret (January–April 2014) allowed explicit representation of canopy and tree temperatures in a three-part subcanopy incoming longwave radiation model (equation (4)), and comparison with the widely used two-part model (equation (3)). The importance of tree trunk temperature can be seen at Tree 2 in Figure 6a, where temperature of the trunk surface was greater than 35°C. Spatial differences in trunk surface temperature can also be seen, some areas of the lower trunk were in excess of 35°C, but the upper tree trunk (more sheltered from direct insolation) and the branches and needles of surrounding trees (smaller thermal capacity) were closer to the measured air temperature (4°C). Differences between measured air temperatures at both Laret and Seehornwald (4 km apart) and tree trunk temperatures at Tree 2 at Laret, are shown in Figure 6b. Air temperatures at Seehornwald were lower than Laret during midday, although at night air temperatures at Seehornwald were between 1 and 3°C higher than at Laret, likely due to the denser forest canopy at Seehornwald reducing turbulent fluxes and energy losses to the atmosphere. Disparities between air and tree temperatures showed different diurnal patterns at Laret compared to Seehornwald (Figures 5 and 6b) due to the different intensities of solar heating at the two field sites—V_f was 0.4 at Laret and <0.18 at Seehornwald. Largest differences between air and tree temperatures at Laret were measured on sunny days with high insolation (e.g., 23 February) while cloudier days had smaller differences (e.g., 17 February) due to reduced solar heating of canopy elements. However, during these cloudy periods tree temperatures remained slightly higher than air temperatures. Temperature differences at Tree 2 (26 February to 11 March) between the trunk and air were smaller than at Tree 1 (8–25 February);

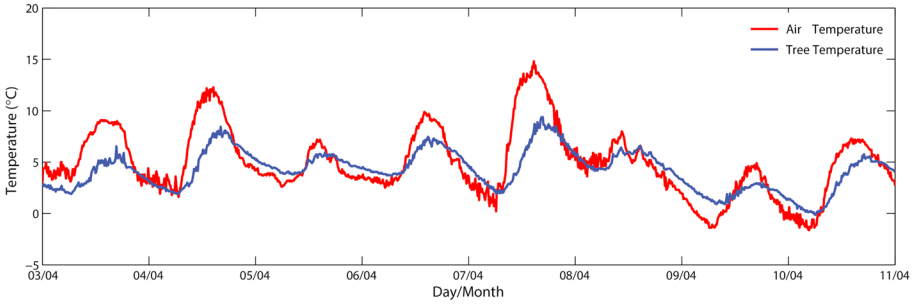

Figure 5. Above-canopy air temperature measured at 35 m and average tree trunk temperature measured between 1 and 3 m above the ground using contact thermocouples at Seehornwald between 3 and 11 April 2014.

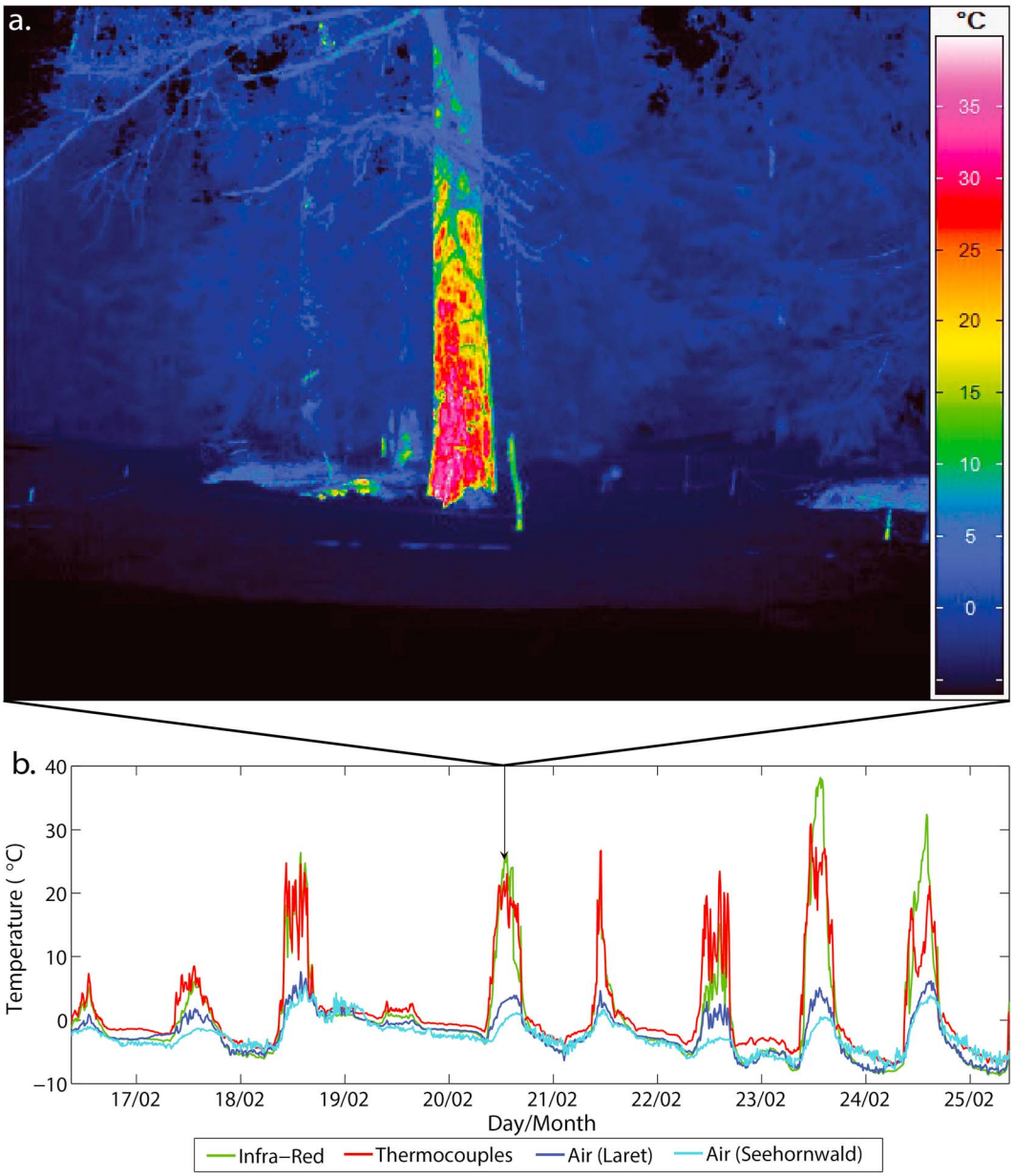

Figure 6. (a) Thermal image taken at 2 P.M. on 20 February 2014 using an emissivity of 1, showing difference between the temperatures of the trunk at Tree 1, surrounding canopy, and snow surface. (b) Air temperatures measured next to the tree at Laret and above the canopy at Seehornwald and tree temperatures using IRTCs and TCs on the south side of Tree 1 from 18 to 25 February. Arrow indicates time and date when the thermal image was taken.

largest difference at Tree 1 was 34°C and 22°C at Tree 2. Furthermore, maximum daytime differences between air and tree temperatures at Tree 2 decreased throughout the snowmelt period; between 16 and 29 April the maximum difference between trunk and air temperatures at Tree 2 was 12°C.

At night the infrared thermocouples measured trunk temperature at Tree 1 similar to the air temperature, whereas the contact thermocouples recorded several degrees warmer (Figure 6b). The temperature difference is likely due to the two instruments measuring either direct surface temperature (IRTCs) or bark temperature several millimeters below the surface (contact TCs). Additionally, the average of the distributed measurements of the contact TCs over the tree trunk (ranging in height from 30 to 150 cm above the snow surface) was warmer than at the base of the trunk where the IRTCs were measuring surface bark temperature. These locations and averaging differences can also explain the different daily patterns in tree trunk temperatures

Table 4. Model RMSE (W m^{-2}) of the Two-Part Model (Equation (3)) at Individual Tree Locations at Laret Using Air Temperature Measured at Seehornwald (SH) and Locally Next to the Tree at Laret (LT)[a]

	Sensor Distance From Tree							
	7 cm (15 cm)		37 cm (30 cm)		67 cm (45 cm)		97 cm (60 cm)	
	SH	LT	SH	LT	SH	LT	SH	LT
Tree 1 installation 1	12.1	9.6	11.2	8.0	8.7	6.0	8.0	5.1
Tree 1 installation 2	21.4	19.3	12.8	11.1	10.2	9.1	8.6	6.9
Tree 2 installation 1	6.2	5.9	6.4	4.0	5.6	4.0	5.5	4.0
Tree 2 installation 2	12.0	8.4	9.9	6.6	11.2	8.4	10.2	7.6

[a]The sensors' distances from the tree during the first installation at Tree 1 (7–20 February) are shown in parentheses.

seen in Figure 6b, where shading of different areas of the tree trunk during the course of the day results in different diurnal patterns of tree temperature between the two instrumental methods.

Air and tree temperatures shown in Figure 6b were used along with V_f and TV_f to calculate incoming longwave radiation using both the two-part and three-part models at both trees in Laret throughout winter 2014. Longwave radiation was modeled at all four different radiometer installations between 7 February and 29 April (Tree 1, installation 1 and 2; Tree 2, installation 1 and 2).

The two-part model performed best at Tree 2 compared to Tree 1 (Table 5); largest RMSE at Tree 1 (installation 2) was 11.5 W m^{-2} compared to 7.0 W m^{-2} at Tree 2 (installation 2). These results were a result of the slightly denser canopy and thus reduced solar heating at Tree 2 compared to Tree 1. Errors in the two-part model were lower during the first installation at Tree 2 compared to the second installation, which can be attributed to lower solar angles earlier in the snowmelt season resulting in less canopy heating. RMSE of the two-part model were higher for the sensors located closest to the tree trunks, with RMSE up to 11.5 W m^{-2} at sensor 1 (7 cm away, $V_f = 0.38$) and 6.7 W m^{-2} at sensor 4 (97 cm away, $V_f = 0.49$). This reduction in error with increasing distance from the tree trunk demonstrates the influence of the heated tree trunk on incoming longwave radiation to the snow surface at closer proximity to tree trunks. The two-part model performed worse during the daytime further demonstrating the effect of the midday solar heating on model bias.

Comparisons between model results using the two-part and three-part models show a reduction in RMSE at all sensors at all four tree installations by the inclusion of TV_f (Tables 4 and 5 and Figure 7). RMSE at Tree 2 ranged from 3.4 to 5.4 W m^{-2} during installation 1 and 6.0 to 7.9 W m^{-2} during installation 2; no pattern was evident between model error and distance from tree trunk. Although there is an improvement by adding trunk temperature to create the three-part model, some variation in estimation of incoming longwave radiation still remains, particularly during installation 2 at Tree 2, suggesting additional processes that are not accounted for in the three-part model. Additionally, when used in the three-part model, neither infrared nor contact thermocouple measurements showed a consistent improvement in model accuracy over one another (Table 5 and Figure 7).

5.3. Predicting Tree Trunk Temperatures

The difference between measured tree trunk temperatures and air temperature showed diurnal variation similar to the pattern of incoming shortwave radiation (Figure 6b), suggesting this difference can be predicted using

Table 5. RMSE (W m^{-2}) of the Three-Part Model (Equation (4)) Using Either Contact Thermocouples (TCs) or Infrared (IRTCs) Measurements of Tree Temperature at the Four Sensors During Winter 2014 at Laret[a]

	Sensor Distance From Tree							
	7 cm (15 cm)		37 cm (30 cm)		67 cm (45 cm)		97 cm (60 cm)	
	TCs	IRTCs	TCs	IRTCs	TCs	IRTCs	TCs	IRTCs
Tree 1 installation 1	3.2	3.8	5.8	6.0	3.7	3.9	3.4	3.6
Tree 1 installation 2	11.5	11.1	6.4	6.4	5.7	5.7	4.2	4.0
Tree 2 installation 1	4.9	5.4	3.5	3.4	3.6	3.5	3.6	3.5
Tree 2 installation 2	5.6	-	3.9	-	4.5	-	4.3	-

[a]The sensors' distances from the tree during the first installation at Tree 1 (7–20 February) are shown in parentheses.

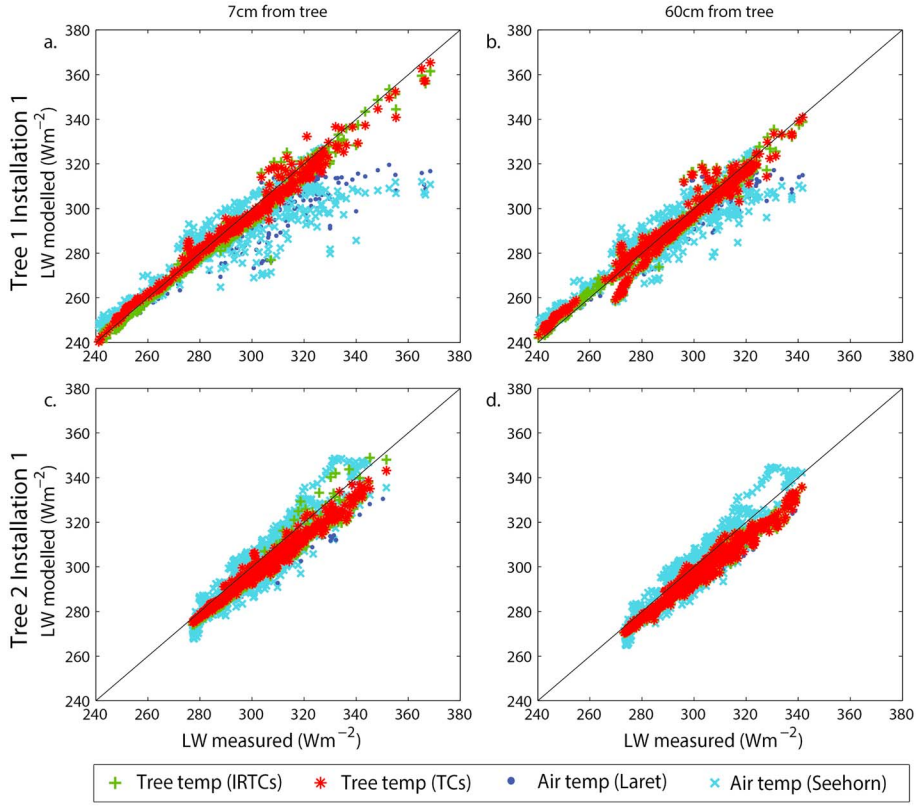

Figure 7. Measured and modeled incoming longwave radiation from the two-part model (equation (3)) using air temperature measured at Laret and Seehornwald and the three-part model (equation (4)) using tree temperatures measured using contact thermocouples (TCs) and infrared thermocouples (IRTCs) (a, b) on the south side of Tree 1 between 10 and 20 February and (c, d) at Tree 2 between 27 February and 13 March using measurements at 7 cm from the tree trunk (Figures 7a and 7c) and 60 cm from the tree trunk (Figures 7b and 7d).

measured incoming shortwave radiation. Initial modeling on individual data from Tree 1 and Tree 2 showed statistically similar relationships between δT and incoming shortwave radiation (t test for model similarity resulted in p value < 0.01). Data from both trees (10 February to 11 March) were combined and used to calculate a simplistic model using local incoming shortwave radiation measured at the base of the tree trunk to predict the difference between air and tree trunk temperatures.

A simple linear model was found to produce the best fit to the data:

$$\delta T = 0.034 * \downarrow \mathrm{SWR} - 1.165 \tag{6}$$

where δT (°C) is $T_{\mathrm{trunk}} - T_{\mathrm{air}}$, $\downarrow$SWR is incoming subcanopy shortwave radiation (W m^{-2}) at the base of the tree trunk. The negative intercept in this model demonstrates air temperature exceeding tree trunk temperature during periods of low incoming shortwave radiation. Furthermore, δT was below 2°C during these periods of low shortwave radiation and there was no clear relationship with δT and subcanopy incoming shortwave radiation, suggesting that during these conditions, air temperature can be used to predict incoming longwave radiation as the assumption suggests.

RMSE of equation (6) was 2.7°C and the fit of the model at each tree is shown in Figure 8a. δT values at Tree 2 were lower than at Tree 1, but overall patterns in δT at each tree were the same. Figure 8b compares modeled incoming longwave radiation using air temperature, measured tree temperature, and predicted tree temperature using equation (6). Model RMSE was reduced from 10.1 W m^{-2} to 8.9 W m^{-2} when using equation (6) to predict tree trunk temperature for the three-part model compared to using air temperature in the two-part model. While improvements were low during periods of low incoming longwave radiation, individual bias values were reduced by up to 20 W m^{-2} during periods of higher incoming longwave radiation when biases from the two-part model were highest (Figure 8b).

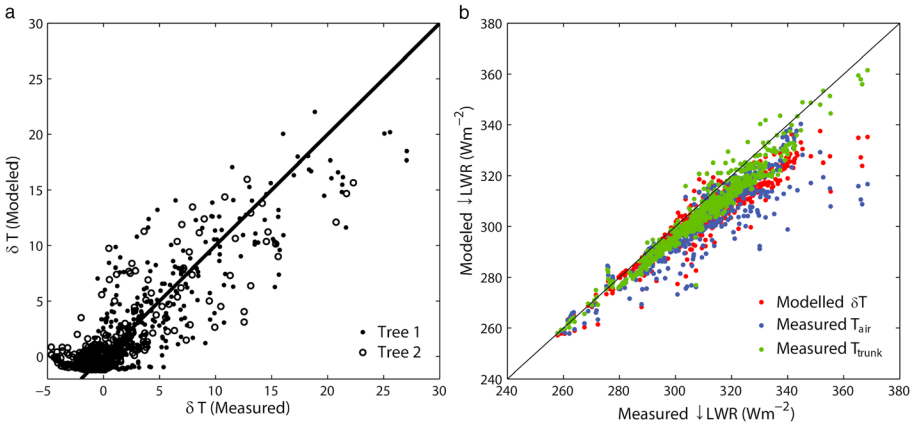

Figure 8. (a) Measured and modeled δT which is $T_{tree} - T_{air}$ from equation (6) using measured air and tree temperatures and incoming shortwave radiation at the base of the tree trunk. (b) Measured and modeled subcanopy incoming longwave radiation using air temperature in the two-part model, measured tree trunk temperature in the three-part model, and modeled tree trunk temperature using equation (6). Data are combined from the radiometer located against the trunk at Tree 1 (7–26 February) and Tree 2 (26 February to 11 March).

6. Discussion

Uncertainties resulting from the use of air temperature to model incoming subcanopy longwave radiation arise due to the vertical temperature variation in the canopy. Vertical air temperature profiles throughout four snow seasons at Alptal (December–April) showed strong differences in measured air temperature between all three measurement heights (2, 10, and 35 m). Consistently lower air temperature measurements at 2 m were indicative of the canopy acting as a sink for cold air throughout the winter/spring period in all four study years, particularly due to the lack of wind and turbulent mixing of air within relatively dense forest canopies [*Link and Marks*, 1999]. These different measurements lead to uncertainties as to which air temperature (above or below canopy) would be best representative of the temperature of the emitting canopy. At the denser Alptal site, the best agreement between modeled and observed subcanopy incoming longwave radiation was obtained when using air temperature measured at 35 m in all 4 years.

In a densely forested environment, *Sicart et al*. [2004] demonstrated that measured above-canopy air temperature showed similarities between the calculated temperature of the emitting canopy below during low sun angles or under cloudy conditions. *Pomeroy et al*. [2009] also found similarities between measured above-canopy air temperature and needle branch temperature, in a midlatitude forest at 2780 m. Data presented in these two studies therefore supports the assumption that measured above-canopy air temperature can be used as a proxy for the effective emitting canopy temperature. However, consistent negative monthly model biases from long-term modeling at Seehornwald demonstrate that using above-canopy air temperature in equation (3) results in a general underestimation of subcanopy incoming longwave radiation particularly during sunny periods, suggesting the temperature of the emitting canopy was higher than air temperature. Overestimations in modeled incoming longwave radiation show that during other periods the above-canopy air temperature were higher than the effective temperature of the emitting canopy.

Tree trunk temperature data from Seehornwald shows that the difference between air and tree temperatures changed from positive to negative throughout a 24 h period. During the day (high insolation) average tree trunk temperature remained lower than above-canopy air temperature; however, individual tree trunk temperatures were as high as 20°C in areas where direct solar radiation reached the tree trunk. These variations in tree trunk and air temperatures demonstrate further limitations in using the two-part model when calculating subcanopy incoming longwave radiation, especially at subdaily times steps.

Overall RMSE values from the two-part model at Seehornwald show that there are periods of time during the day when air temperature and the effective emitting canopy temperature are similar. These low individual bias values thus reduce the overall model RMSE, even though there are times when model bias is $>15\,W\,m^{-2}$. Furthermore, periodic overestimation and underestimation suggest a compensation effect in the calculation of model bias, where the underestimations during sunny periods cancel out overestimations during other periods,

thus reducing overall model bias. This compensation is likely to have led to the lower model bias values using above-canopy air temperatures compared to within (10 m) and below (2 m) canopy temperatures at Alptal, which were overall too cold to represent solar heating of the canopy.

Wider implications for model over and underestimations in subcanopy longwave radiation, by using above-canopy air temperatures in the two-part model, can be seen when considering the results of *Lundquist et al.* [2013]; regions experiencing December–February temperatures (>1°C) led to winter melt events and earlier snow melt out in the forest compared to the open due to longwave radiation emitted by the forest canopy. The use of a "surface" temperature in snowmelt and land surface models [e.g., *Best et al.*, 2011], whether measured above the canopy, within the canopy, or at an open site, would lead to incorrect estimations of modeled melt rates and snow disappearance dates in the forest compared to open sites. These errors would be particularly prevalent in more topographically complex environments, where vertical and horizontal spatial variations in air temperature are larger and slope and aspect variations affect net incoming radiation [*Ellis et al.*, 2011].

Point-scale modeling at Laret showed improvement on the widely used two-part air temperature model by adding measured TV_f and trunk temperature to create the three-part model. The underestimation of modeled longwave radiation by the two-part model, particularly at Tree 1 could be improved first by the use of a local within canopy air temperature compared to an above-canopy temperature measured at Seehornwald, and also the incorporation of the TV_f and trunk temperature to create the three-part model. These improvements were particularly evident when measured subcanopy incoming longwave radiation was higher than 310 W m^{-2}, when air temperatures were above 0°C. Despite evident improvements using the three-part model instead of the two-part model, the reduction in model RMSE was within the range of the error of the pyrgeometers (±10%). However, while improvements were small during periods of low incoming longwave radiation, individual bias values were reduced by up to 25 W m^{-2} during periods of maximum daily incoming longwave radiation.

Large errors in the two-part model during maximum daily incoming longwave radiation could also be improved by predicting tree trunk temperature using equation (6) and measured air temperature. Equation (6) demonstrates a simple method to calculate tree trunk temperatures when air temperature and subcanopy incoming shortwave radiation data are available. Similarities between the parameterization at both Tree 1 and Tree 2 suggest that this parameterization can be applied over further midlatitude alpine coniferous forests, although recalculation is likely required in other latitudes and forest types. This model is most useful during clear-sky conditions when incoming solar radiation and subcanopy incoming longwave radiation are at a maximum. Therefore, when subcanopy data are unavailable, there is potential for this model to be applied using modeled subcanopy shortwave radiation, for example, using ray tracing [*Musselman et al.*, 2015] or lidar and hemispherical photography [*Moeser et al.*, 2014].

Previous modeling work has only used theoretical TV_f and measured tree temperature [*Pomeroy et al.*, 2009] or simply used air temperature, shortwave radiation, or an untested relationship between the two [*Lawler and Link*, 2011; *Seyednasrollah and Kumar*, 2013, 2014]. Incorporating measured or modeled TV_f and trunk temperature to create a three-part model of subcanopy incoming longwave radiation (equation (4)) reduces the RMSE compared to the two-part model (equation (3)) at all sensor positions close to tree trunks (7–97 cm) throughout the 2014 snowmelt season at Laret. The three-part model improves the greatest closer to the tree trunks (within 1 m), a proximity that is important because it is in these areas of the forest where snowmelt initiates against tree trunks and creates a preferential melt profile [*Woo and Giesbrecht*, 2000], and where model error with the two-part model is highest [*Lawler and Link*, 2011]. Further away from these heated tree trunks, the trunk view component decreases and the heated tree trunks have less influence on the radiation budget at the snow surface. This suggests the two-part model can work sufficiently in the center of forest gaps where V_f is high [*Lawler and Link*, 2011; *Seyednasrollah and Kumar*, 2014]. Consequently, prediction of snowmelt initiation and evolution is therefore dependent on accurate representations of the tree trunk and its temperature, which can be better achieved by accounting for canopy and tree trunk temperatures when modeling subcanopy incoming longwave radiation.

Despite its improvement to subcanopy incoming longwave radiation prediction close to tree trunks, the three-part model is currently only applicable for point-scale modeling where trunk view fraction is manually determined from hemispherical photographs, and tree trunk temperature can be measured only at a small number of specific trees using infrared or contact thermocouples. Methods to measure forest and tree temperatures across a wider scale are required in order to increase the accuracy of incoming longwave radiation

modeling across larger areas. While a measurement of the trunk view component might not be possible across larger forested areas, recent developments in airborne lidar data of forested areas have calculated canopy components such as mean distance to tree and canopy gap size [*Moeser et al*., 2015; *Varhola and Coops*, 2013; *Varhola et al*., 2010]. However, application of this forest structure data to larger-scale modeling requires distributed temperature data to further improve incoming longwave radiation modeling estimates at the landscape scale.

7. Conclusions

This study used data collected during the snowmelt season at three different Swiss subalpine forested sites over a combined period of 11 years to evaluate the use of air and tree trunk temperature in modeling subcanopy incoming longwave radiation. Errors in the widely used two-part model were shown to arise from the assumption that the air temperature can be used as a proxy for the canopy temperature. Vertical variations in air temperature through the canopy at Alptal resulted in different estimations of subcanopy incoming longwave radiation modeled using three different temperatures (2, 10, and 35 m). Subcanopy (2 m) air temperature was the coldest and above-canopy (35 m) temperatures were the warmest, suggesting the presence of the canopy acts as a sink for cold air. The above-canopy temperatures had the lowest RMSE when modeling subcanopy incoming longwave radiation throughout four studied years (2004–2007). Further investigation at Seehornwald between 2008 and 2014 showed that using above-canopy air temperature as a proxy for the canopy temperature resulted in general overestimations of subcanopy longwave radiation and underestimations during periods of higher insolation. These results demonstrate a need for incorporating canopy temperatures into the subcanopy incoming longwave model. Measured trunk view fraction and trunk temperature were included in the widely used two-part model, partitioning the hemispherical view into three components to create a three-part model. The three-part model was tested at sensors located within 1 m of tree trunks at Laret during winter 2014 and was shown to reduce the RMSE of the simple two-part air temperature model at all sensors by up to 7.7 W m^{-2}. A simple model was developed to allow prediction of tree trunk temperature if direct measurements are unavailable, instead using measured air temperature and incoming subcanopy shortwave radiation. This model should be applicable across midlatitude coniferous forests and the method could further be used in other forested areas following a recalibration of the model using site-specific measurements.

Acknowledgments

The authors would like to acknowledge Bruno Fritschi for the development, construction and maintenance of the rail structure and radiation measurements at Alptal and Seehornwald. Temperature data from the towers were provided by Patrick Schleppi (Alptal) and the National Air Pollution Monitoring Network (NABEL) (Seehornwald). Data used within this study are available upon request. Funding for the CMP3 and CGR3 radiometers used in this study was provided from the UK's Natural Environment Research Council (NERC) grant NE/H008187/1. We would also like to thank Jessica Lundquist and one other anonymous reviewer whose comments have helped improve this paper.

References

Best, M. J., et al. (2011), The Joint UK Land Environment Simulator (JULES), model description—Part 1: Energy and water fluxes, *Geosci. Model Dev.*, *4*(3), 677–699, doi:10.5194/gmd-4-677-2011.

Chang, M. (2003), *Forest Hydrology: An Introduction to Water and Forests*, CRC Press, Boca Raton, Fla.

Ellis, C., J. Pomeroy, T. Brown, and J. MacDonald (2010), Simulation of snow accumulation and melt in needleleaf forest environments, *Hydrol. Earth Syst. Sci. Discuss.*, *7*(1), 1033–1072.

Ellis, C., J. Pomeroy, R. Essery, and T. Link (2011), Effects of needleleaf forest cover on radiation and snowmelt dynamics in the Canadian Rocky Mountains, *Can. J. For. Res.*, *41*(3), 608–620.

Essery, R., J. Pomeroy, C. Ellis, and T. Link (2008), Modelling longwave radiation to snow beneath forest canopies using hemispherical photography or linear regression, *Hydrol. Processes*, *22*(15), 2788–2800.

Flerchinger, G., W. Xaio, D. Marks, T. Sauer, and Q. Yu (2009), Comparison of algorithms for incoming atmospheric long-wave radiation, *Water Resour. Res.*, *45*, W03423, doi:10.1029/2008WR007394.

Fröhlich, C. (1977), World radiometric reference, Commission for Instruments and Methods of Observation. Abridged final report of the seventh session, CIMO-VII, WMO(490).

Gouttevin, I., M. Lehning, T. Jonas, D. Gustafsson, and M. Mölder (2015), A two-layer canopy with thermal inertia for an improved modelling of the sub-canopy snowpack energy-balance, *Geosci. Model Dev. Discuss.*, *8*(1), 209–262, doi:10.5194/gmdd-8-209-2015.

Gubler, S., S. Gruber, and R. S. Purves (2012), Uncertainties of parameterized surface downward clear-sky shortwave and all-sky longwave radiation, *Atmos. Chem. Phys.*, *12*(11), 5077–5098, doi:10.5194/acp-12-5077-2012.

Harding, R., and J. Pomeroy (1996), The energy balance of the winter boreal landscape, *J. Clim.*, *9*(11), 2778–2787.

Hardy, J., R. Davis, R. Jordan, W. Ni, and C. E. Woodcock (1998), Snow ablation modelling in a mature aspen stand of the boreal forest, *Hydrol. Processes*, *12*(1011), 1763–1778.

Howard, R., and R. Stull (2013), IR radiation from trees to a ski run: A case study, *J. Appl. Meteorol. Climatol.*, *52*(7), 1525–1539, doi:10.1175/jamc-d-12-0222.1.

Lawler, R. R., and T. E. Link (2011), Quantification of incoming all-wave radiation in discontinuous forest canopies with application to snowmelt prediction, *Hydrol. Processes*, *25*(21), 3322–3331.

Link, T. E., and D. Marks (1999), Point simulation of seasonal snow cover dynamics beneath boreal forest canopies, *J. Geophys. Res.*, *104*(D22), 27,841–27,857.

Liston, G. E., and K. Elder (2006), A meteorological distribution system for high-resolution terrestrial modeling (MicroMet), *J. Hydrometeorol.*, *7*(2), 217–234.

Lundquist, J. D., S. E. Dickerson-Lange, J. A. Lutz, and N. C. Cristea (2013), Lower forest density enhances snow retention in regions with warmer winters: A global framework developed from plot-scale observations and modeling, *Water Resour. Res.*, *49*, 6356–6370, doi:10.1002/wrcr.20504.

Marks, D., and J. Dozier (1992), Climate and energy exchange at the snow surface in the Alpine Region of the Sierra Nevada: 2. Snow cover energy balance, *Water Resour. Res.*, *28*(11), 3043–3054, doi:10.1029/92WR01483.

Moeser, D., J. Roubinek, P. Schleppi, F. Morsdorf, and T. Jonas (2014), Canopy closure, LAI and radiation transfer from airborne lidar synthetic images, *Agric. Forest Meteorol.*, *197*, 158–168.

Moeser, D., F. Morsdorf, and T. Jonas (2015), Novel forest structure metrics from airborne lidar data for improved snow interception estimation, *Agric. Forest Meteorol.*, *208*, 40–49, doi:10.1016/j.agrformet.2015.04.013.

Musselman, K. N., J. W. Pomeroy, and T. E. Link (2015), Variability in shortwave irradiance caused by forest gaps: Measurements, modelling, and implications for snow energetics, *Agric. Forest Meteorol.*, *207*, 69–82, doi:10.1016/j.agrformet.2015.03.014.

Pomeroy, J. W., D. Marks, T. Link, C. Ellis, J. Hardy, A. Rowlands, and R. Granger (2009), The impact of coniferous forest temperature on incoming longwave radiation to melting snow, *Hydrol. Processes*, *23*(17), 2513–2525, doi:10.1002/hyp.7325.

Price, A., and D. Petzold (1984), Surface emissivities in a boreal forest during snowmelt, *Arct. Alp. Res.*, *16*, 45–51.

Reid, T., and R. Essery (2013), New methods to quantify canopy structure of leafless boreal birch forest from hemispherical photographs, *Open J. For.*, *3*, 70.

Rowlands, A., J. Pomeroy, J. Hardy, D. Marks, K. Elder, and R. Melloh (2002), Small-scale spatial variability of radiant energy for snowmelt in a mid-latitude sub-alpine forest, paper presented at Proceedings of the 59th Eastern Snow Conference.

Seyednasrollah, B., and M. Kumar (2013), Effects of tree morphometry on net snow cover radiation on forest floor for varying vegetation densities, *J. Geophys. Res. Atmos.*, *118*, 12,508–12,521, doi:10.1002/2012JD019378.

Seyednasrollah, B., and M. Kumar (2014), Net radiation in a snow-covered discontinuous forest gap for a range of gap sizes and topographic configurations, *J. Geophys. Res. Atmos.*, *119*, 10,323–10,342, doi:10.1002/2014JD021809.

Sicart, J. E., R. L. H. Essery, J. W. Pomeroy, J. Hardy, T. Link, and D. Marks (2004), A sensitivity study of daytime net radiation during snowmelt to forest canopy and atmospheric conditions, *J. Hydrometeorol.*, *5*(5), 774–784, doi:10.1175/1525-7541(2004)005<0774:assodn>2.0.co;2.

Sicart, J. E., J. W. Pomeroy, R. L. H. Essery, and D. Bewley (2006), Incoming longwave radiation to melting snow: Observations, sensitivity and estimation in Northern environments, *Hydrol. Processes*, *20*(17), 3697–3708, doi:10.1002/hyp.6383.

Stähli, M., T. Jonas, and D. Gustafsson (2009), The role of snow interception in winter-time radiation processes of a coniferous sub-alpine forest, *Hydrol. Processes*, *23*(17), 2498–2512.

Varhola, A., and N. C. Coops (2013), Estimation of watershed-level distributed forest structure metrics relevant to hydrologic modeling using lidar and Landsat, *J. Hydrol.*, *487*, 70–86, doi:10.1016/j.jhydrol.2013.02.032.

Varhola, A., N. C. Coops, C. W. Bater, P. Teti, S. Boon, and M. Weiler (2010), The influence of ground-and lidar-derived forest structure metrics on snow accumulation and ablation in disturbed forests, *Can. J. For. Res.*, *40*(4), 812–821.

Webster, C., N. Rutter, F. Zahner, and T. Jonas (2015), Measurement of incoming radiation below forest canopies: A comparison of different radiometer configurations, *J. Hydrometeorol.*, doi:10.1175/JHM-D-15-0125.1.

Woo, M.-k., and M. A. Giesbrecht (2000), Simulation of snowmelt in a subarctic spruce woodland: 1. Tree model, *Water Resour. Res.*, *36*(8), 2275–2285, doi:10.1029/2000WR900094.